# African Journal of Advanced Pure and Applied Sciences (AJAPAS)

*Online ISSN: 2957-644X*

Volume 3, Issue 1, January-March 2024, Page No: 193-209

Website: *https://aaasjournals.com/index.php/ajapas/index*

**معامل التأثير العربي 2023: (1.55)** **SJIFactor 2023: 5.689** **ISI 2022-2023: 0.557**


# Development of Barkhausen Noise Method for Residual Stress Evaluation In Steels


Osama Hamed Abd Alsalam Alasamar *

Department of Electric and Electronic Engineering, College of Technical Sciences Sebha, Sebha, Libya

*Corresponding author: osamaalasmar@gmail.com



| Received: January 22, 2024 | Accepted: March 01, 2024 | Published: March 13, 2024 |
|---|---|---|



**Abstract:**

A significant amount of the hysteresis in the magnetization of a ferromagnetic material takes place with a random chain of discontinuous motions of magnetic domain walls. This gives rise to what is called Magnetic Barkhausen Noise (MBN). These noise events are analysed statistically during the detection of the random voltage monitored on a pickup coil through the magnetization of the material. The study of Magnetic Barkhausen Noise (MBN) can provide information on the interaction between stress and domain walls arrangements, or composition or microstructure. The method is a complementary Non-Destructive Testing (NDT) procedure to that of eddy-current inspection. This article will focus on the effect of stress on Magnetic Domain configuration, and how this is reflected in the Magnetic Barkhausen Noise (MBN) signal, and how it can be analyzed by using a diversity of parameters. Simultaneously, residual stresses and dislocations take part in an important function in the Magnetic Barkhausen Noise (MBN) investigation, complementary the analysis and adding to the competitiveness of Magnetic Barkhausen Noise (MBN) as a Non-Destructive Testing (NDT) technique for ferromagnetic materials. This article will also focus on Grinding, Grinding Burn and its various types, and compare with other residual stress detection methods particularly the X–Ray Diffraction Method (XRD).



**Keywords**: Magnetic Barkhausen Noise, Non-Destructive Testing, X–Ray Diffraction Method, Residual Stresses.

**Cite this article as:** O. H. A. Alasamar, "Development of Barkhausen Noise Method for Residual Stress Evaluation In Steels," *African Journal of Advanced Pure and Applied Sciences (AJAPAS)*, vol. 3, no. 1, pp. 193–209, January-March 2024.




# تطوير طريقة ضوضاء باركهاوزن لتقييم الإجهاد المتبقي في الفولاذ


أسامة حامد عبد السلام الاسمر *

قسم الهندسة الكهربائية والإلكترونية، كلية العلوم التقنية سبها، ليبيا



**الملخص**

يحدث قدر كبير من التباطؤ في مغنطة مادة مغناطيسية حديدية من خلال سلسلة عشوائية من الحركات المتقطعة لجدران المجال المغناطيسي. وهذا يؤدي إلى ما يسمى بضوضاء باركهاوزن المغناطيسية (MBN). يتم تحليل أحداث الضوضاء هذه إحصائيًا أثناء اكتشاف الجهد العشوائي الذي يتم مراقبته على ملف الالتقاط من خلال مغنطة المادة. يمكن أن توفر دراسة ضوضاء باركهاوزن المغناطيسية (MBN) معلومات حول التفاعل بين ترتيبات الإجهاد وجدران المجال، أو التركيب أو البنية المجهرية. الطريقة عبارة عن إجراء اختبار غير مدمر (NDT) مكمل لإجراء فحص التيار الدوامي. ستركز هذه المقالة على تأثير الضغط على تكوين المجال

المغناطيسي، وكيف ينعكس ذلك في إشارة ضوضاء باركهاوزن المغناطيسية(MBN) ، وكيف يمكن تحليلها باستخدام مجموعة متنوعة من المعلمات. في الوقت نفسه، تلعب الضغوط والاضطرابات المتبقية دورًا مهمًا في تحقيق ضوضاء باركهاوزن المغناطيسي(MBN) ، حيث تكمل التحليل وتضيف إلى القدرة التنافسية لضوضاء باركهاوزن المغناطيسية (MBN) كتقنية اختبار غير مدمر (NDT) للمواد المغناطيسية الحديدية. ستركز هذه المقالة أيضًا على الطحن وحرق الطحن وأنواعه المختلفة، والمقارنة مع طرق الكشف عن الإجهاد المتبقي الأخرى وخاصة طريقة حيود الأشعة السينية (XRD) .

**الكلمات المفتاحية:** ضوضاء باركهاوزن المغناطيسية، الاختبارات غير المتلفة، طريقة حيود الأشعة السينية، الإجهادات المتبقية.

## Introduction

The evaluation of residual stress in steels is crucial for ensuring the structural integrity and performance of components and structures [1]. Residual stress arises from various manufacturing processes such as welding, heat treatment, and machining, and it can significantly affect the mechanical properties and fatigue life of steel materials [2]. Traditional methods for residual stress measurement often involve destructive techniques or require extensive sample preparation. However, the Barkhausen noise method has emerged as a promising non-destructive approach for evaluating residual stress in steels [3]. In this article, we will explore the development of the Barkhausen noise method and its application in the assessment of residual stress in steel materials [4].

Steels and other ferromagnetic materials can have their magnetic characteristics and microstructure evaluated non-destructively using the Barkhausen noise method [5]. It bears Heinrich Barkhausen's name, a German physicist who made the initial observation of the phenomena in the early 1900s. The technique is predicated on the idea that an alternating magnetic field applied to a ferromagnetic material causes the material's magnetic domains to alter in magnetic alignment. Barkhausen noise is the name for the tiny, distinct magnetic energy bursts that are released as a result of these changes [6].

The main contribution of the article is. While the remining section are organized as follows: The methodology that using two methods (Influence of Grain Size and Influence of Compositional and Phase) are presented in Section 2. Section 3 discussing the materials as Grinding along with its classifications. Section 4 replaced the utilized equipment's for Barkhausen Noise. The obtained results discussed in Section 5 followed with it discussion for the three samples. Finaly, the article closed by the summary of conclusion in Section 6 and list of recent references.

## Methodology

### Effects of Microstructure on Magnetic Barkhausen Noise (MBN)

#### Influence of Grain Size

MBN signal is strongly affected by the number of grain boundaries which are directly related to the average grain sizes (a larger number of boundaries is found in samples with smaller grains). The boundaries act as sources for domain wall pinning, leading to large number of grain boundaries resulting in higher MBN signal [7].

If uniaxial stress is applied, the magnetic domain structure will be changed, however, only magnetic domains that are separated by non-$180^{\circ}$domain walls will be affected [3]. Additionally, number of $180^{\circ}$domain walls will be changed, if stress is sufficiently large enough. This value depends on the grain size and increases with the number of existing domain walls. Therefore, this also confirms that MBN signal is strongly affected by the grain size and grain boundaries [8].

Additionally, precipitates and segregation at grain boundaries can act as additional pinning sites for domain walls, which increases the number of MBN signal [9]. Also, agglomerations of dislocations at grain boundaries act as additional pinning sites as well, increasing the MBN signal [10].

#### Influence of Compositional and Phase

Interpretation of MBN analysis becomes more difficult if compared between the samples with different composition or phase changes can bring their own contribution to signals, causing the MBN analysis to be more complicated. For example, changes of the carbon content in plain carbon steels make distinctive change in MBN signal due to increase of pinning of domain walls by volumes of carbide phase [11].

## Grinding

### Grinding mechanisms

As this article is related to the study of ground surfaces of the samples a brief introduction to the grinding process is presented. Removal of material surface together with honing, lapping and polishing is called grinding. This machining process involves interaction of hard abrasives with the material at high cutting speeds and low penetration depths, resulting in removal of the material surface [12].

As shown in Fig**ure** 1, there are five main elements that affect grinding: (i) Grinding wheel which does the machining, (ii) Material which is subjected to grinding, Grinding fluid which serves three purposes: (iii) coolant for the material, remover of swarf and lubricator at the contact zone, (iv) Grinding swarf which is a

combination of cut chips from the material, the grinding fluid and worn abrasives from the wheel, and, finally, (v) Atmosphere [13].

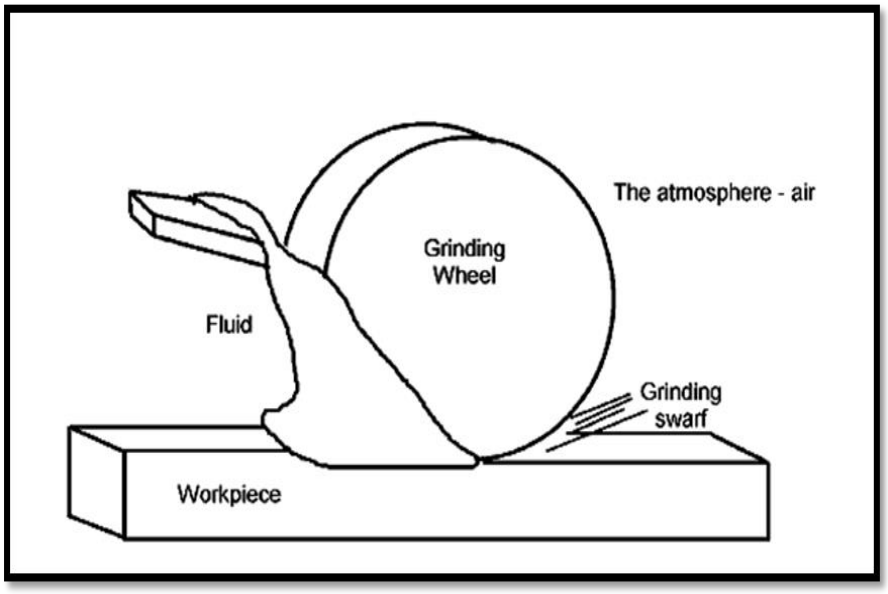


**Figure. 1:** Five important elements of a typical grinding process.

Overall, grinding can be divided into three mechanisms based roughly on penetration depth of the abrasive grain. Rubbing, with smallest penetration depth, is based on simple friction but still causes some elastic and material deformation. Ploughing, with slightly bigger penetration depth, causes scratches and ridges to the material. Cutting is the mechanism with the biggest penetration depth. The energy from the first two mechanisms goes into the material in the form of heat, and the energy from the third mechanism goes with grinding swarf [14]. The penetration depth of the abrasive grinding is therefore controlling the amount of damage to the materials surface.

Additionally, the atmosphere also affects the amount of damage to the materials surface in a form of oxidation layer. This layer in the contact zone is illustrated in Fig**ure**. 2 [15].

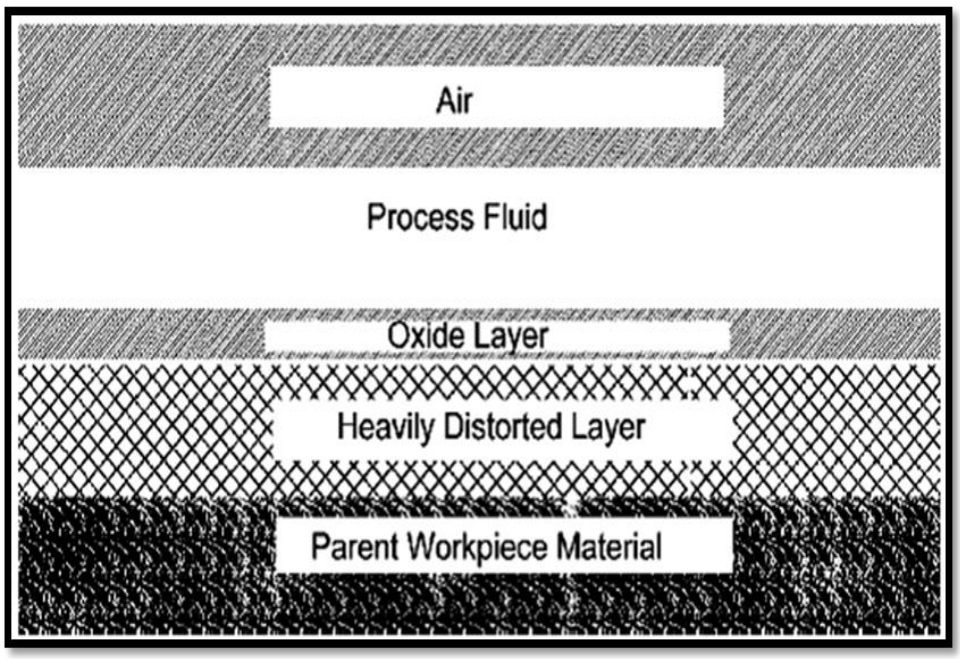


**Figure 2:** Various Interaction layers in contact zone during grinding process.

**Grinding Burn and its Types**

Due to high temperature occurring during the grinding process, metallurgical damage in the form of high tensile residual stress, phase changes or even cracks in the material occur, which is termed grinding burn [16]. This causes microstructural softening with lower hardness. This is called a Temper Burn (over tempered martensite OTM). On the other hand, if the material was overheated during grinding and then rapidly quenched, this induces re-hardening burn damage and is called Re-Hardening Burn (untampered martensite UTM). This results in near surface layer that has an unacceptably high hardness and compressive residual stress.

Finally, the presence of a small amount of OTM or UTM will cause a significant reduction in the fatigue strength of the material.

**X–ray Diffraction (XRD) Method to Estimate Residual Stresses**

Residual stresses can be divided into Macrostresses (stresses averaged over several grains) and Microstresses (stresses over a single grain or stresses on atomic level) (see Fig**ure**. 3). X-ray diffraction and Neutron diffraction are examples of destructive methods of evaluating stresses compared to the non-destructive MBN and ultrasonics techniques [17].

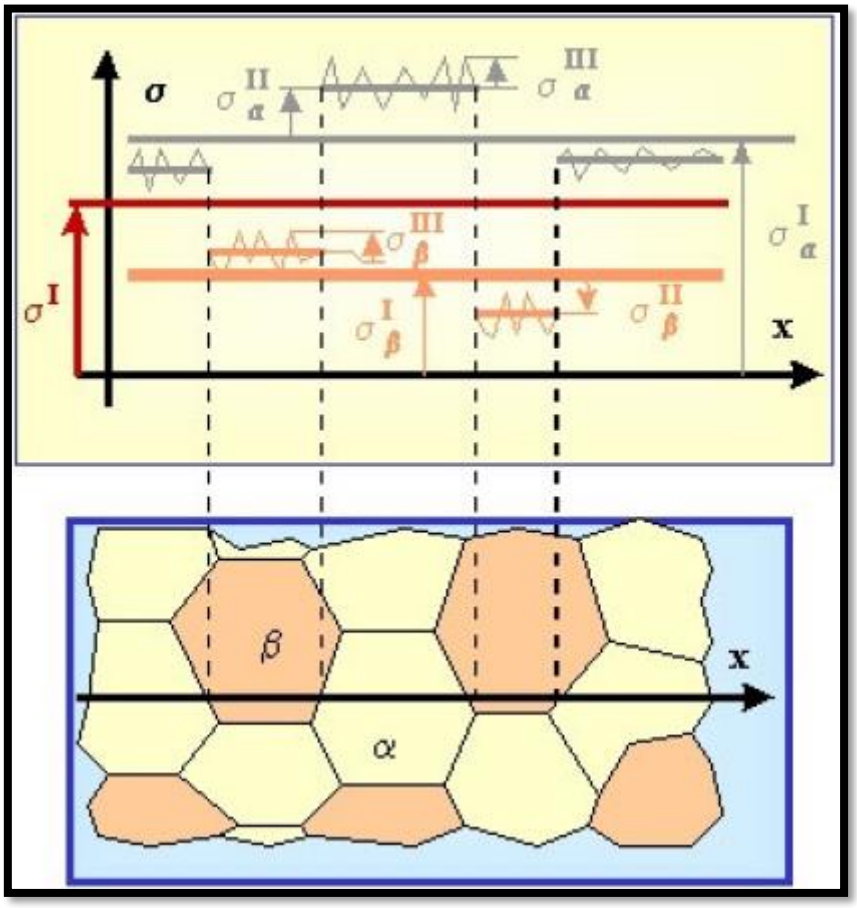


**Figure 3:** Macrostresses (marked as I) and Microstresses (marked as II and III) residual stress can be

As this article will use the results of the X–ray diffraction measurements, therefore, the X–ray diffraction method is briefly explained. The X–ray diffraction method is a well-established, standard method widely used by industry and can identify residual stresses and phase characterisations of materials (internal stresses, grain size, phase composition etc). Its principle relies on the fact that the residual stresses affect lattice spacing.

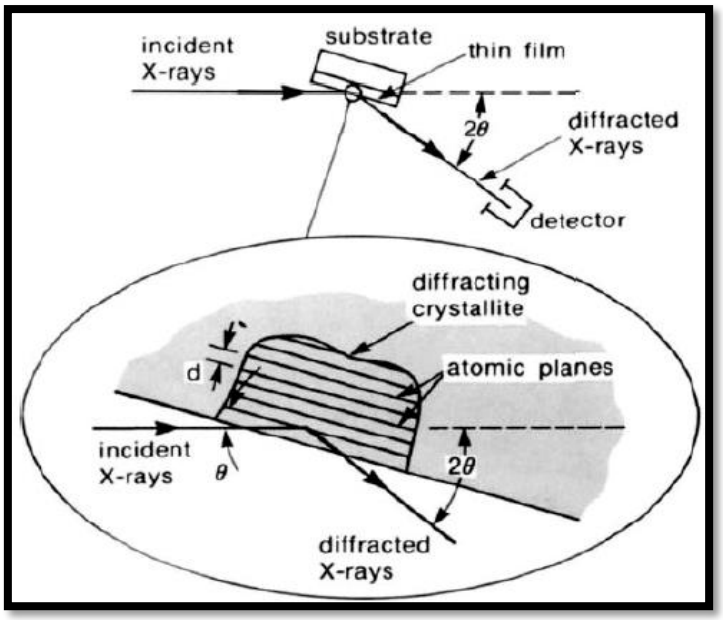


**Figure 4:** Basic features of a typical XRD experiment.

The change in lattice spacing will be seen as a change in a diffraction spectrum and thus can be identified using Bragg's Eq.1:

$$\mathbf{n\lambda = 2dsin\theta} \qquad 1$$

where **n is** an integer corresponding to the order of diffraction, λ is the wavelength of the diffracted x – ray radiation, and θ is the angle of incidence of the crystal plane. Measuring the lattice spacing (as shown in Fig**ure** 4) and knowing the elastic modulus allow estimation of the value of residual stress [49,

Among other methods to estimate the residual stresses are Neutron diffraction and ultrasonics, for example. Neutron diffraction is similar to XRD, but neutrons are used instead of X–rays as they give a greater depth penetration (0.2mm to 25mm for steels) compared to X–rays [18]. Ultrasonic method, on the other hand, is a non-destructive method which uses the fact that the velocity of ultrasonic wave is a function of a residual stress, therefore, measuring the velocity of ultrasonic wave, the residual stress can be estimated.

**MicroScan 600 Unit and Software used for Barkhausen Noise**

**Equipment**

The Barkhausen Noise measurements were conducted at Wolfson Centre for Magnetics, School of Engineering, Cardiff University using a MicroScan 600 made by Stresstech Oy/American Stress Technologies (AST) (see Fig**ure** 5). These instruments are sophisticated and easily adjustable and are widely used as Non-Destructive Testing (NDT) systems [19]. Some NDT applications include identifying Barkhausen Noise changes due to change in microstructure, detection of residual stresses at surfaces, estimation of gradients of stress or hardness, and other application and general research work [20].

Fig**ure** 5 illustrates MicroScan 600 connected with standard PC computer, the system used in Wolfson Centre for Magnetics. The standard PC computer controls the magnetising current and analyses the output using specialised commercial software.

The sensor head of the MicroScan 600 unit consists of the yoke and the pickup device. The MicroScan 600 unit creates a sinusoidally varying current, which is supplied to a coil wound around a yoke Fig**ure** 7. The yoke is then put on top of the sample and a pickup coil, wound around a core, acquires the MBN voltage signal, which is amplified and filtered and saved for further post-processing. Good care has to be taken to ensure that there is a good contact between both yoke and core of the sensor (Fig**ure**. 8) and the surface of the sample [19].

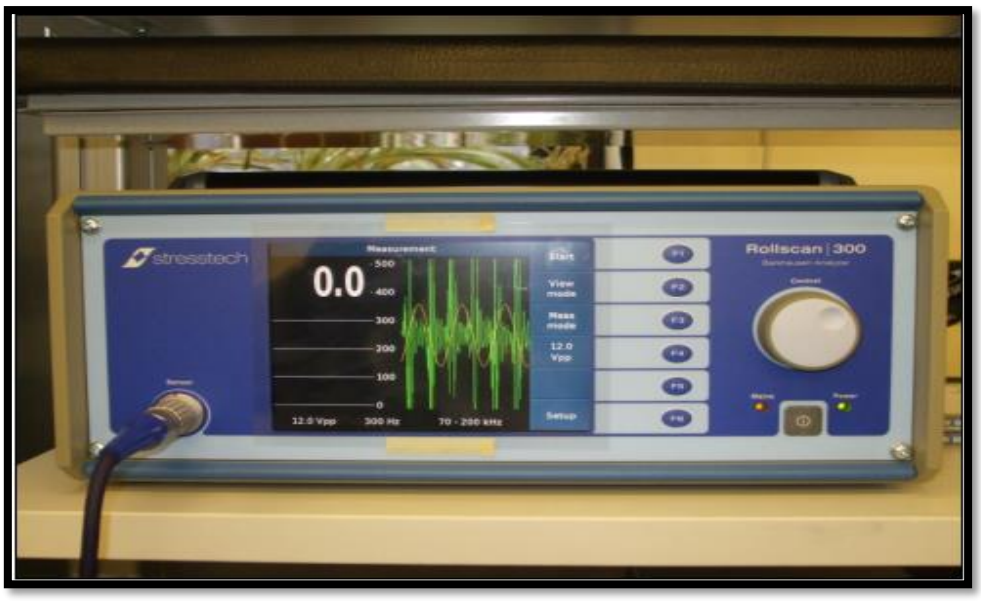


**Figure 5:** Barkhausen Noise Testing Unit.

**Figure 6:** Illustrates MicroScan 600 connected with Computer.

The MicroScan 600 unit can be controlled by the user through the software, where all measurement parameters are controlled, and the results are calculated and displayed. Additionally, the parameters used to analyse the MBN results can be extracted for adjustable analyzing frequency interval, allowing characterisation of near surface gradients like stress, plastic deformation, hardness, etc. [20].

The parameters of measurements which can be controlled through the software are [20]:

- **Magnetising frequency: 6…300 Hz**
- **Magnetising voltage: 1…16 V**
- **No of bursts: 1…20**
- **Sampling frequency: maximum 2500 kHz**
- **Range of analysing frequency: 0.1…1250 kHz**
- **Smoothing parameter: 1…100**

Where Magnetizing Frequency and Voltage are used to produce **AC** magnetic field and Number of Burst means number of half magnetizing cycles. Sampling Frequency means how many "samples" or measurement per second are stored for analysis of signals, for example, how detailed signal a "snapshot" will be. (Alternatives are 2.5 MHz and 1MHz). Because the pace high to avoid distortion of the signal. It is well known that elements of the signal of a higher frequency of 500 kHz to 1 MHz sampling could be used. Use only 2.5 MHz is strongly suggested because of the conflict that may happen with HW-filters and 1 MHz sampling frequency. Analysing Frequency range is selected in kHz. In higher or maximum range $\mathbf{f_s}$ is the frequency of sampling. Altering analyzing frequency range allows changing the depth from which BN information is coming lower the frequency the larger the depth. And finally, the smoothing is for the smoothing number to control the scatter in the envelope curve. Smoothing is made by moving average method [20].

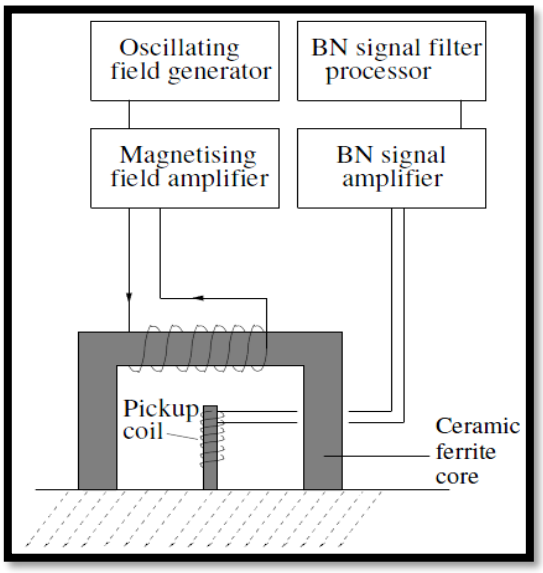


**Figure 7:** Schematic diagram of MicroScan 600 unit.

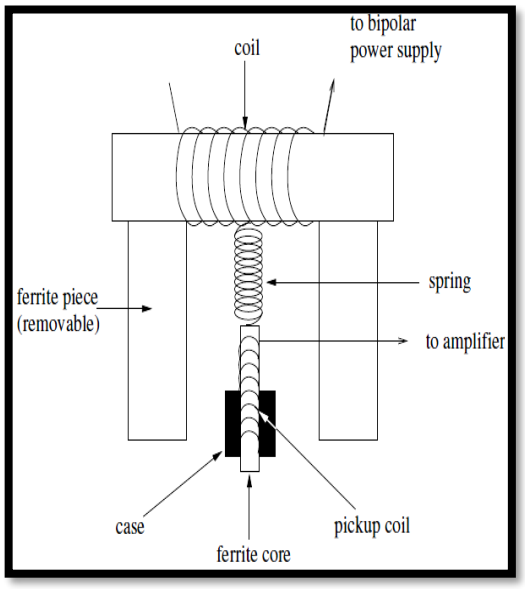


**Figure 8:** Schematic diagram of the sensor of the MicroScan 600 unit.

**Procedure to Measure Magnetic Barkhausen Noise (MBN) using MicroScan 600 unit**

The equipment used in this work in order to measure the MBN signal was MicroScan 600 made by Stresses Oy/American Stress Technologies (AST).

First, the control parameters for the MBN readings had to be set up using the control software of the MicroScan 600. For example, the software measurement parameters used to measure the samples in this article are shown in Fig**ure**. 9.

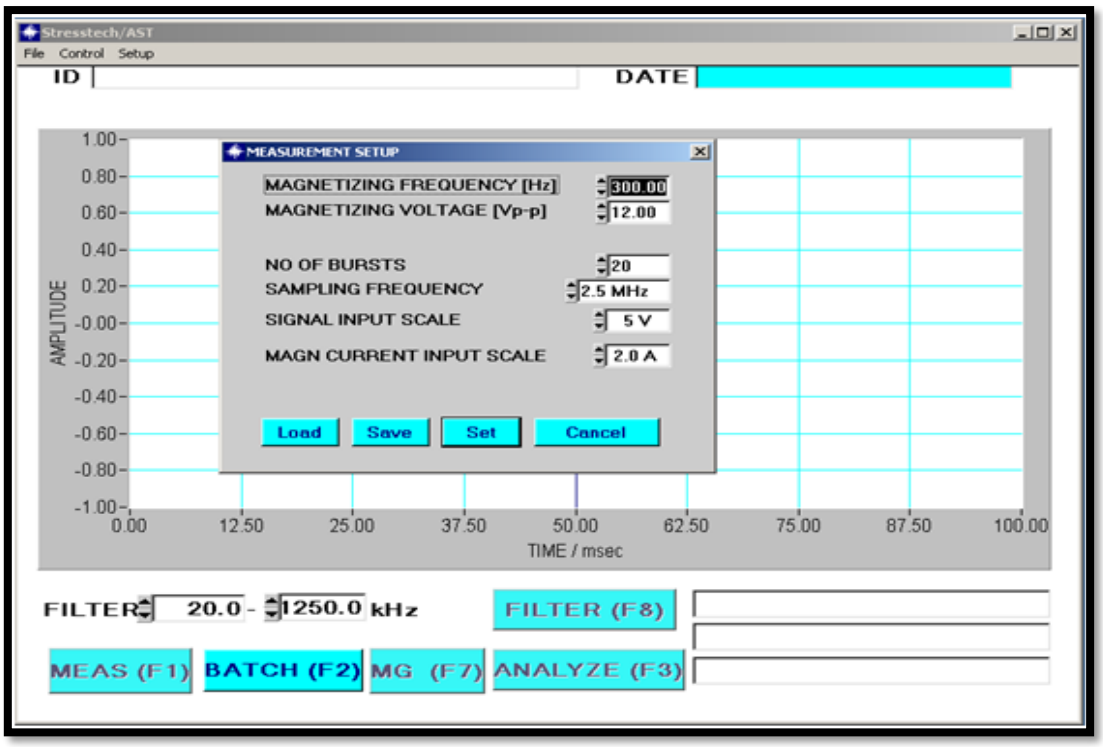


**Figure 9:** Measurement parameters set in MicroScan software.

After that the sensor was put on the surface of the sample making sure that there is no gap between sensor and surface of the sample in order to allow maximum flux flow from the yoke into the sample (see Fig**ure**. 10). When the measurement parameters were set up and the sensor was placed on the top of the sample, the readings were taken.

**Figure 10:** Measuring the MBN signal of a sample.

The resultant MBN signal is shown in the display of the MicroScan 600 unit and is also saved by the software (Figure. 11) for subsequent analysis (Figure. 12) within the software.

For example, the segments of positive and negative for the 4 bursts are shown in Fig**ure**. 11. The green curve is the requirement magnetising current, and the red curve is a parabola fitted to the first half of the session. The Red curve is not appropriate on the curve of magnetising current means a saturation of the sensor's magnetising circuit and the measurements have to be taken again, then recalibration will be done automatically by software.

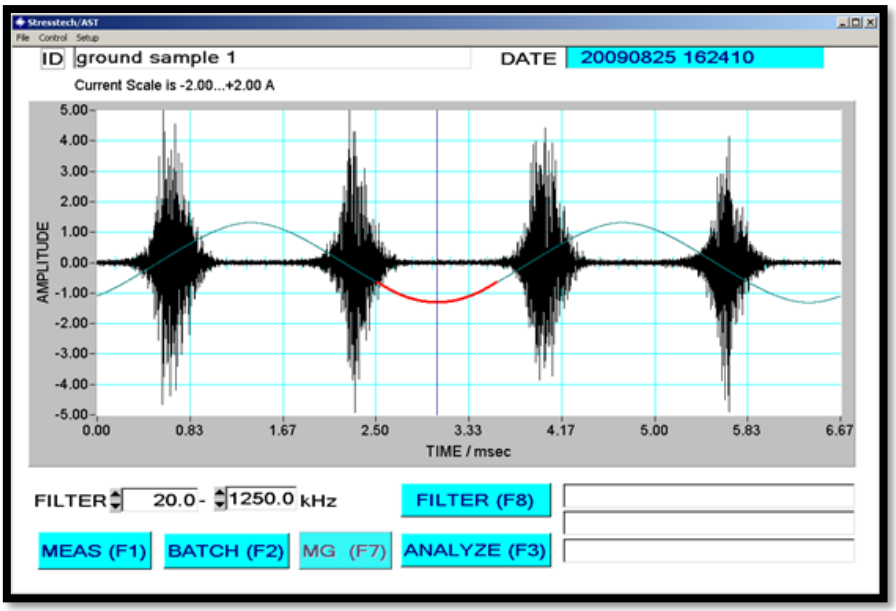


**Figure 11:** Principal window of MicroScan with captured MBN signal

The MicroScan software provides the analysis of the measured MBN signal and extracts the parameters used in the analysis. The extraction of the parameters for this study is shown in Fig**ure** 12:

- **RMS Voltage of the Barkhausen noise (V rms)**
- **Peak Voltage (V peak)**
- **Peak Position**
- **Full Width Half Maximum (FWHM)**
- **Permeability**

These parameters are investigated over the range of frequencies from 20 kHz to 1250 kHz. Further analysis of these parameters could allow determination of residual stress at different depths below the surface of the sample, if the range of frequencies is varied. However, this current project excludes this complicated analysis.

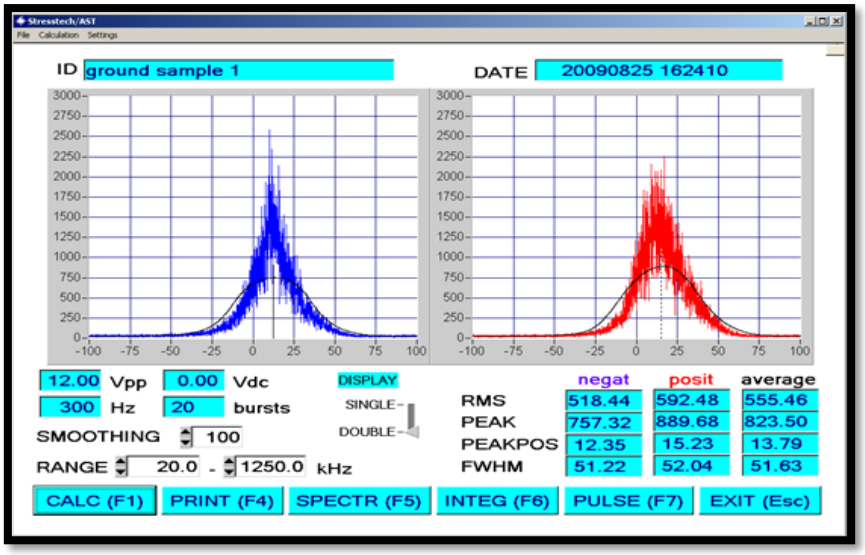


**Figure 12:** Analyse window with a little calculated parameter.

**Results and discussion**
**Description of Samples and Barkhausen Noise Measurement**
**Results for Samples with Different Grades of Grinding Burns**

The samples which were selected and used in this article consist of 3.25%NiCrMo Case Hardening Steel Single Melted or Vacuum Arc Remelted (VAR) and provided by Agusta Westland. The Table 1 below shows the chemical composition.

**Table 1:** Samples Chemical Composition (Wt %).

| | Min | Max |
|---|---|---|
| C | **0.07** | **0.13** |
| Si | **0.15** | **0.35** |
| Mn | **0.40** | **0.70** |
| P | **-** | **0.015** |
| S | **-** | **0.015** |
| Cr | **100** | **1.40** |
| Mo | **0.08** | **0.15** |
| Ni | **3.00** | **3.50** |
| B | **-** | **0.001** |
| Cu | **-** | **0.35** |

The properties and advantages of these samples are: - middle-strength steel (1150 MPa), excellent in the property's browser, VAR material develops a hard ware resistance after the state surface treatment. Among the material applications are: Aircraft industry with heavy load bearing components of helicopters, and fishing gear, and as load bearing Transmissions. The material can be Heat Treated: Case hardened. Quenched and tempered [56]. Some properties are illustrated in Table 2 after a specific heat treatment.

**Table 2:** Mechanical Properties after concluding heat treatment.

| Direction | 0.2% Proof Stress MPa | Tensile Strength MPa | Elongation % | Reduction of area % | Hardness HRC |
|---|---|---|---|---|---|
| | **Min** | **Min** | **Min** | **Min** | |
| Longitudinal | **900** | **1150** | **14** | **65** | **36** |
| Transverse | **900** | **1150** | **8** | **40** | |

The samples which were used in the measurement in this article were in the form of cylinders with the dimensions as illustrated in Fig**ure**. 13 below, these samples provided by Augusta Westland, and the depth of the layer removed in a grinding process was approximately 0.5 mm.

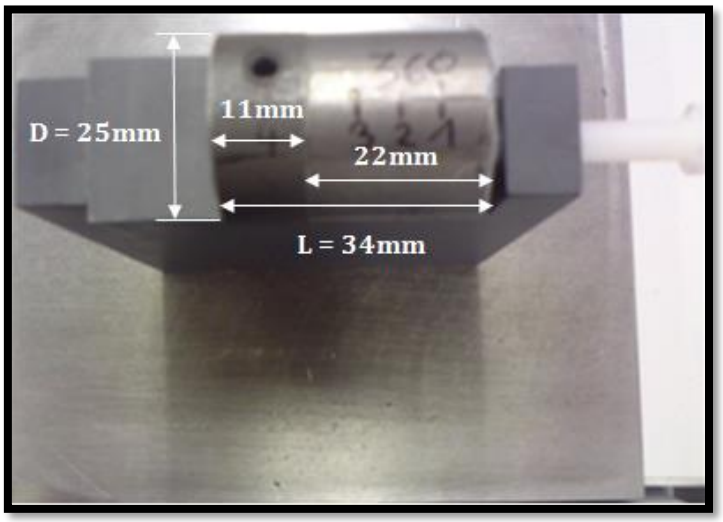


**Figure 13:** Illustrates the dimensions on the sample.

Inspection locations for Barkhausen measurements were marked and numbered around the circumference at angles of **90, 180, 270, 360** degrees and along the length of the sample as illustrated in Fig**ure**. 14, and all chosen samples have different stress profiles as illustrated in Fig**ure**. 15, Fig**ure**. 17 and Fig**ure**. 19 provided by Agusta Westland. The deeper stress profiles for all three samples are attached in Appendixes.

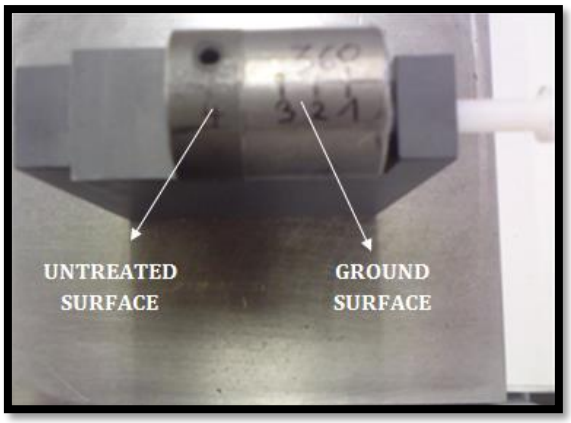


**Figure 14:** Illustrates inspection locations on the sample.

This section of the article contains results from Magnetic Barkhausen Noise measurements for three samples (marked as Sample 1, 2 and 3) which were selected to represent various effects of abusive grinding on microstructure and residual stress. The following magnetising and analysis parameters were used as listed in Table 3.

**Table 3:** Results of Magnetic Barkhausen Noise measurements

| Parameters | Values |
|---|---|
| Magnetising frequency: | f = 300 Hz |
| Magnetising voltage: | V = 12 V |
| No of bursts: | #cycles = 20 |
| Range of analysing frequency: | fa = (20…1250) kHz |
| Smoothing parameter: | sp = 100 |
| Sampling frequency: | fs =2,5MHz. |

Finally, the resulting envelope curves for initial and ground surfaces for each sample are illustrated in Fig**ure** 16, Fig**ure**. 18 and Fig**ure**. 19. Each ground curve in those Figures is constructed using averaging of the three inspection locations along the sample as shown in Fig**ure**. 14 and Table 4.

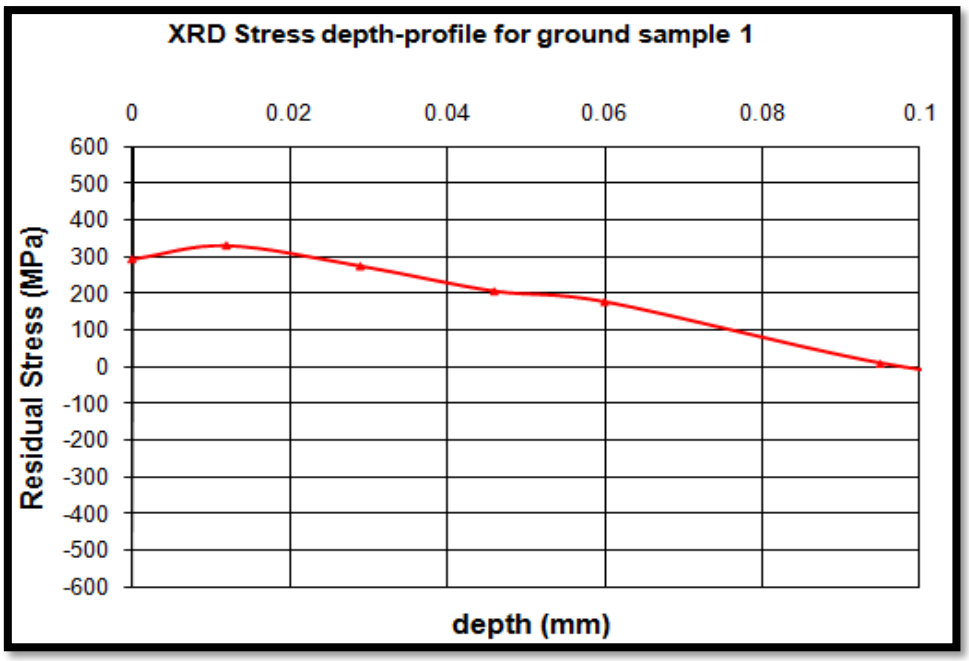


**Figure 15:** XRD depth profile for sample 1. Provided by Agusta Westland

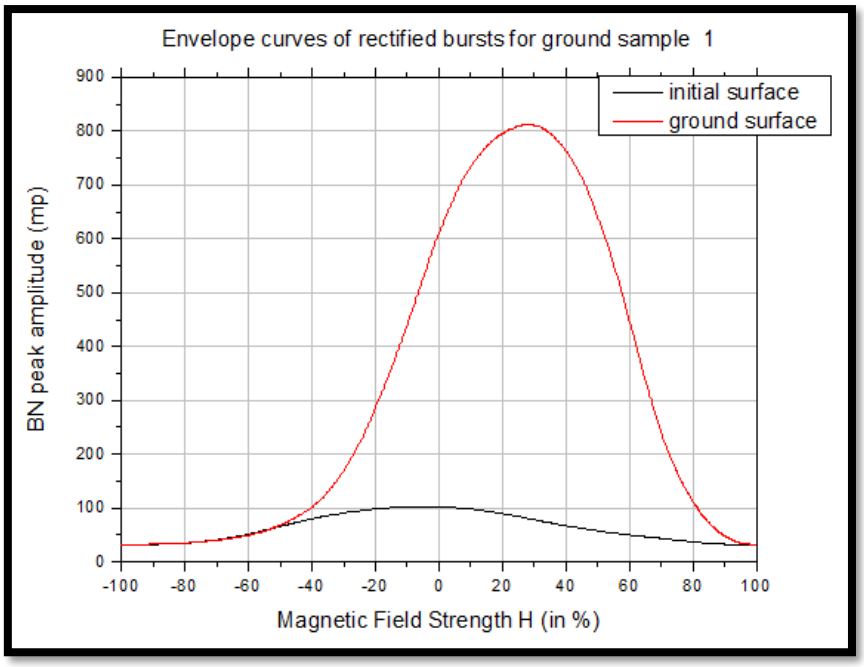


**Figure 16:** Comparison of averaged Barkhausen envelope curves of the rectified bursts for sample 1

**Table 4:** Summary of MBN parameters for sample 1

| | Ground Surface | Initial surface |
|---|---|---|
| BN RMS Average | 555.526 | 76.705 |
| BN Peak Average | 813.418 | 101.205 |
| BN Pos Average | 16.921 | -2.574 |
| BN FWHM Average | 51.433 | 61.375 |

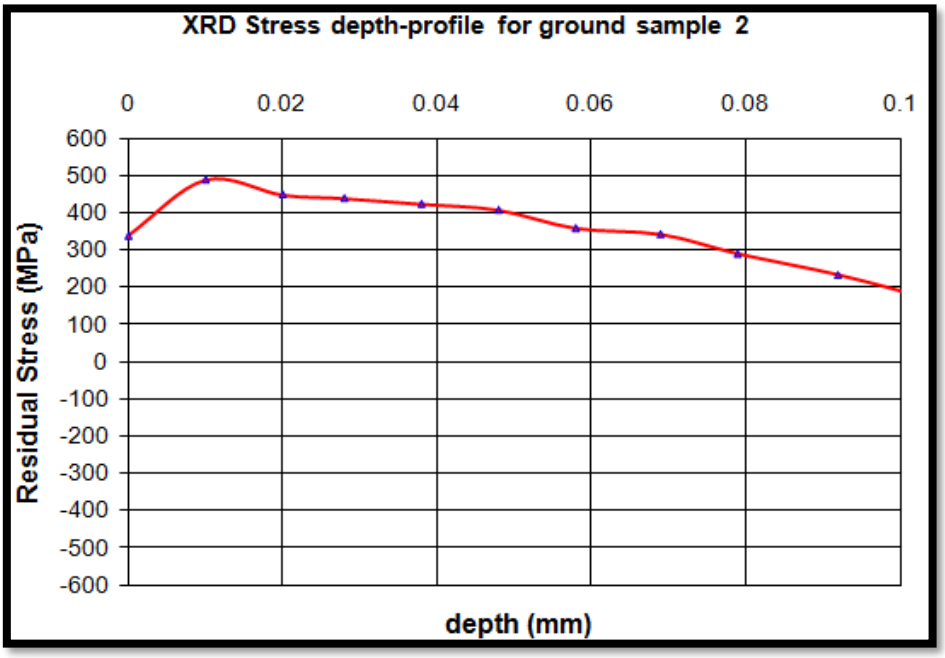


**Figure 17:** XRD depth profile for sample 2. Provided by Agusta Westland**.**

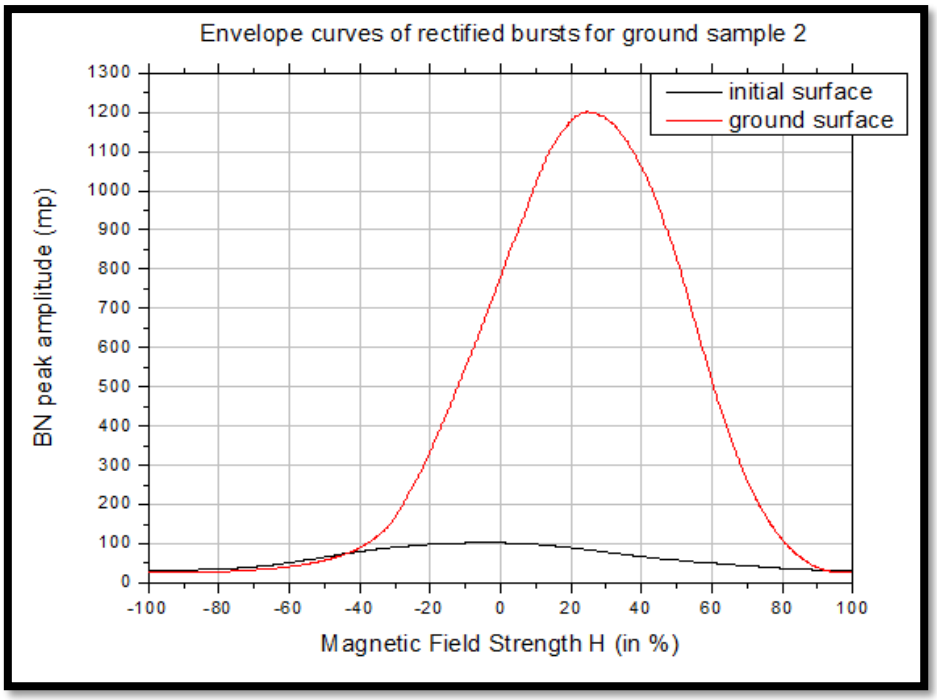


**Figure 18:** Comparison of averaged Barkhausen envelope curves of the rectified bursts for sample 2

**Table 5:** Summary of MBN parameters for sample 2

| | Ground Surface | Initial surface |
|---|---|---|
| BN RMS Average | **787.9825** | **74.3625** |
| BN Peak Average | **1173.904** | **97.26** |
| BN Pos Average | **17.9375** | **-2.8085** |
| BN FWHM Average | **51.8275** | **63.3** |

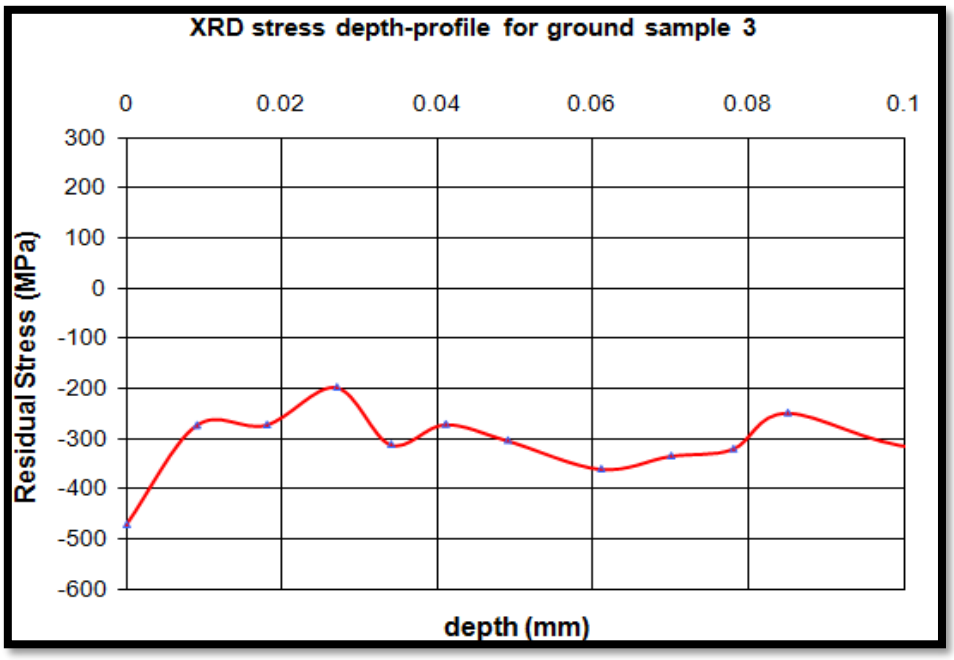


**Figure 19:** XRD depth profile for sample 3. Provided by Agusta Westland**.**

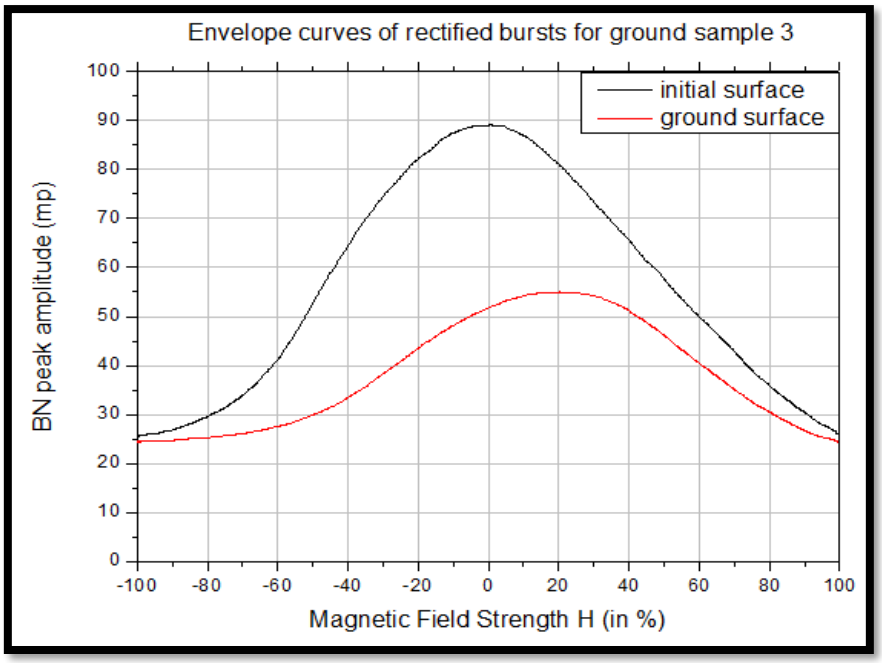


**Figure 20:** Comparison of averaged Barkhausen envelope curves of the rectified bursts for sample 3

**Table 6:** Summary of MBN parameters for sample 3

| | Ground Surface | Initial surface |
|---|---|---|
| BN RMS Average | **49.24** | **72.2275** |
| BN Peak Average | **55.29125** | **85.6275** |
| BN Pos Average | **13.9375** | **-0.13225** |
| BN FWHM Average | **64.1225** | **65.6525** |

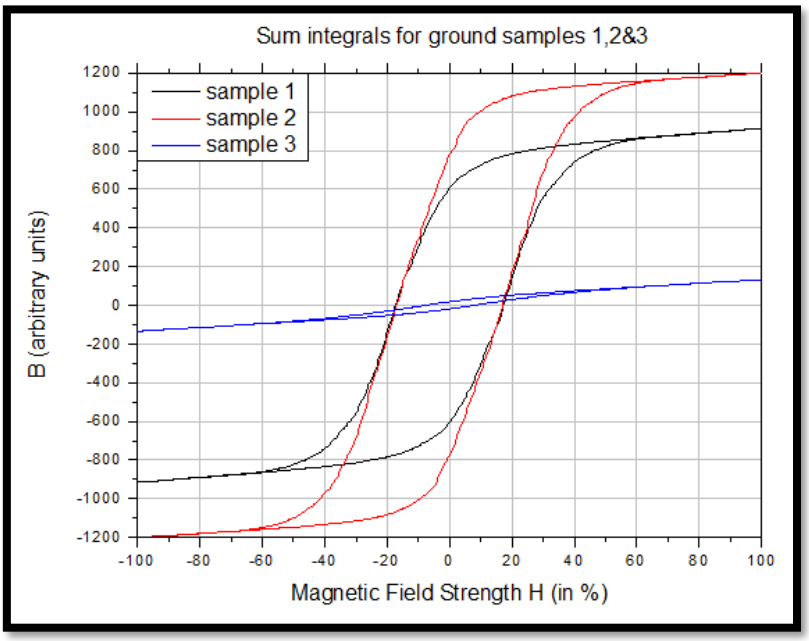


**Figure 21:** Illustrates sum integrals for sample 1, 2 and 3

**Discussion**

MBN results for all the samples demonstrate that the differences in the grinding process can have different effects on mechanical and magnetic properties.

Barkhausen Noise results clearly indicate that there are two distinguishable regions on the surface of **sample 1.**

- Initial surface **(Untreated Surface)** which has not been ground
- Side surface **(Ground Surface)** after grinding.

As can be observed from Fig**ure** 16 the peak positions occur for different values of magnetising current for two curves. If we consider that magnetizing current ***I*** is directly proportional to the applied magnetic field ***H*** and the position of peak amplitudes of Barkhausen noise corresponds to coercive field point $H_C$ where the differential permeability is the highest, then we can assume that low values of peak position indicate a soft magnetic layer (low coercivity, low hardness) and high values of peak position indicates a hard magnetic layer (high coercivity, high hardness).

In practice any change in the location of the peak position of the Barkhausen noise indicates an alteration in the microstructure and hardness in the surface layers of tested material.

In this case the peak position reveals the difference between a harder side surface layer (with a peak occurring at high field value) and a softer initial layer (with a peak occurring at low field values).

These regions seem to have different hardness peak location and magnitude of residual stress peak amplitude which can be observed in Fig**ure** 16.

The "initial" surface had the lowest Barkhausen amplitude, therefore the most compressive stress and its peak occurs at approximately **-10%** of the maximum magnetizing current, and hence at **-10%** of the maximum field amplitude.

It is also shown in Fig**ure**. 16 that peak position of Barkhausen activity for the side surface shifted to the right **30%** meaning an increased magnetising field was needed compared to the initial surface value. This suggests that this layer is harder. The higher BN peak amplitude on this side surface compared with the "initial" surface indicates the presence of tensile stress in the surface and near subsurface.

**Sample 2** was selected in order to demonstrate the differences in the grinding process can have different influence on mechanical and magnetic properties.

It is also shown in Fig**ure** 18 that peak position of Barkhausen activity for the side surface shifted to the right **28%** meaning an increased magnetising field was needed compared to the initial surface value. This also suggests that this layer is harder. The higher BN peak amplitude on this side surface compared with the "initial" surface indicates the presence of tensile stress in the surface and near subsurface.

However, if we compare Fig**ure** 16 and Fig**ure** 18 there was no difference in initial surface peak amplitude, because the value was similar between them, but at side surface there was different peak position, and peak position shifted from left to right, which means coercivity increased and mechanical hardness increased as well.

**Sample 3** is representative of this group of samples for which the grinding process might have caused an increase in hardness of the side surface in comparison with its primary state. This change was indicated by the shift of the BN peak position to a higher value of excitation current, and hence a higher field as shown in Fig**ure**. 20.

The decrease in BN Peak value might imply variation in residual stress magnitude which probably became more compressive. The XRD profile for this sample confirms the presence of the desirable compressive stress state in the surface and near subsurface.

Comparing the samples 1, 2 and 3 we find the sample 3 is "better" than samples 1 and 2, because XRD profile for sample 3 confirms the presence of desirable compressive stress in the surface, while in samples 1 and 2 the XRD profile confirms they have tensile stress, which is not desirable as it can result in crack growth in the surface leading to mechanical failure.

## Conclusion

The development of the Barkhausen noise method has provided a valuable non-destructive technique for the evaluation of residual stress in steels. Through calibration, sensitivity analysis, and validation studies, researchers have established the correlation between the Barkhausen noise signal and residual stress levels. The method's non-destructive nature, cost-effectiveness, and wide applicability make it a practical tool for assessing residual stress in various steel components and structures, contributing to improved quality control, safety, and performance in engineering applications.

Thermomechanical damage caused by abusive grinding, which is characterised as grinding burn, can be present in different forms in the surface layers of these steels.

Results of Barkhausen Noise measurements obtained for Samples 1, 2 and 3 with different grades of abusive grinding have illustrated that it is possible to detect and distinguish regions with differences in hardness and residual stress state in the surface and near subsurface layers. Higher levels of tensile stress cause an increase in Barkhausen signal amplitude, while compressive stress reduces the amplitude. On the other hand, increased hardness as a result of grinding damage increases the field at which the peak in Barkhausen activity occurs, while decreased hardness causes a reduction in the field at which the peak occurs.

These results illustrate that Magnetic Barkhausen Noise tests can be applied non-destructively and can reveal various forms of damage including:

- The formation of a hard brittle layer (a “white” layer) during re-hardening burn associated with formation of tensile stresses present in the side surface layer of sample 1

Overall, therefore, the Barkhausen inspection method seems to have capability for detecting differences in mechanical conditions of the surfaces of steels, and in particular can detect the presence of undesirable tensile stress in the surface and can distinguish this from variations in surface hardness.

**Reference**


[1] L. Schaper, T. Tankova, M. Knobloch, and L. S. da Silva, “A Novel Residual Stress Model for Welded I-sections and the Influence on the Stability Behaviour,” ce/papers, vol. 5, no. 4, pp. 370–377, Sep. 2022, doi: 10.1002/cepa.1767.

[2] J. Wu, H. Liu, P. Wei, Q. Lin, and S. Zhou, “Effect of shot peening coverage on residual stress and surface roughness of 18CrNiMo7-6 steel,” Int. J. Mech. Sci., vol. 183, p. 105785, Oct. 2020, doi: 10.1016/j.ijmecsci.2020.105785.

[3] P. Fagan, B. Ducharne, L. Daniel, and A. Skarlatos, “Multiscale modelling of the magnetic Barkhausen noise energy cycles,” J. Magn. Magn. Mater., vol. 517, p. 167395, Jan. 2021, doi: 10.1016/j.jmmm.2020.167395.

[4] B. Ducharne, Y. A. Tene Deffo, P. Tsafack, and S. H. Nguedjang Kouakeuo, “Directional magnetic Barkhausen noise measurement using the magnetic needle probe method,” J. Magn. Magn. Mater., vol. 519, pp. 1–30, 2021, doi: 10.1016/j.jmmm.2020.167453.

[5] J. Di, “Multigradient Characterization of the Strain in Low-Carbon Steel Components Based on Magnetic Barkhausen Noise Method,” IEEE Sens. J., vol. 24, no. 4, pp. 4334–4342, Feb. 2024, doi: 10.1109/JSEN.2023.3347668.

[6] P. Huang, P. Zhang, S. Xu, H. Wang, X. Zhang, and H. Zhang, “Recent advances in two-dimensional ferromagnetism: materials synthesis, physical properties and device applications,” Nanoscale, vol. 12, no. 4, pp. 2309–2327, 2020, doi: 10.1039/C9NR08890C.

[7] M. R. Neyra Astudillo, N. M. Núñez, M. I. López Pumarega, G. Ferrari, J. Ruzzante, and M. Gómez, “Study of martensite induced by deformation with Magnetic Barkhausen Noise technique,” J. Magn. Magn. Mater., vol. 556, p. 169454, Aug. 2022, doi: 10.1016/j.jmmm.2022.169454.

[8] Y. Liu, Z. Ma, X. Liu, and Z. Zhang, “Effect of grain size and grain boundary on ductile to brittle transition behavior of Fe-6.5wt.%Si alloy under miniaturized three-point bending tests,” Mater. Lett., vol. 353, p. 135288, Dec. 2023, doi: 10.1016/j.matlet.2023.135288.

[9] J. Gao et al., “Grain boundary co-segregation of B and Ce hindering the precipitates of S31254 super austenitic stainless steel,” J. Mater. Res. Technol., vol. 24, pp. 2653–2667, 2023, doi: 10.1016/j.jmrt.2023.03.135.

[10] T. T. H. Nguyen et al., “Understanding the agglomerate crystallisation of hexamine through X-ray microscopy and crystallographic modelling,” J. Cryst. Growth, vol. 603, no. July 2022, p. 126986, 2023, doi: 10.1016/j.jcrysgro.2022.126986.

[11] T. Lambert et al., “Design and first operation of the MACARON irradiation experiment of Sodium Fast reactor absorber pins in the BOR-60 reactor,” Prog. Nucl. Energy, vol. 135, p. 103676, May 2021, doi: 10.1016/j.pnucene.2021.103676.

[12] Z. Tang, W. Liu, N. Zhang, Y. Wang, and H. Zhang, “Real–time prediction of penetration depths of laser surface melting based on coaxial visual monitoring,” Opt. Lasers Eng., vol. 128, p. 106034, May 2020, doi: 10.1016/j.optlaseng.2020.106034.

[13] R. L. Rodriguez et al., “Evaluation of grinding process using simultaneously MQL technique and cleaning jet on grinding wheel surface,” J. Mater. Process. Technol., vol. 271, no. March, pp. 357–367, 2019, doi: 10.1016/j.jmatprotec.2019.03.019.

[14] A. Beaucamp, B. Kirsch, and W. Zhu, “Advances in grinding tools and abrasives,” CIRP Ann., vol. 71, no. 2, pp. 623–646, 2022, doi: 10.1016/j.cirp.2022.05.003.

[15] M. Wang, J. Zhang, H. Zou, Z. Huang, and L. Zhang, “Constructing an ideal home: Affective atmosphere creation as a public participation strategy for urban village renovation,” Cities, vol. 146, p. 104777, Mar. 2024, doi: 10.1016/j.cities.2023.104777.

[16] B. He, C. Wei, S. Ding, and Z. Shi, “A survey of methods for detecting metallic grinding burn,” Measurement, vol. 134, pp. 426–439, Feb. 2019, doi: 10.1016/j.measurement.2018.10.093.

[17] J. Merz, D. Cuskelly, A. Gregg, A. Studer, and P. Richardson, “On the complex synthesis reaction mechanisms of the MAB phases: High-speed in-situ neutron diffraction and ex-situ X-ray diffraction studies of MoAlB,” Ceram. Int., vol. 49, no. 23, pp. 38789–38802, Dec. 2023, doi: 10.1016/j.ceramint.2023.09.216.

[18] Q. Ma, Y. Cao, X. Ge, Z. Zhang, S. Gao, and J. Song, "X-Ray Excited Luminescence Materials for Cancer Diagnosis and Theranostics," Laser Photon. Rev., vol. 18, no. 2, Feb. 2024, doi: 10.1002/lpor.202300565.

[19] V.Jászfi et al., "Indirect yoke-based B-H hysteresis measurement method determining the magnetic properties of macroscopic ferromagnetic samples part I: Room temperature," J. Magn. Magn. Mater., vol. 560, p. 169655, Oct. 2022, doi: 10.1016/j.jmmm.2022.169655.

[20] D. S. Molodenskiy, D. I. Svergun, and A. G. Kikhney, "Artificial neural networks for solution scattering data analysis," Structure, vol. 30, no. 6, pp. 900-908.e2, Jun. 2022, doi: 10.1016/j.str.2022.03.011.